Electronic Supplementary Material (ESI) for ChemComm.
This journal is © The Royal Society of Chemistry 2016

Electronic Supplementary Information (ESI)

Remarkably colorimetric sensing of heavy metal ions based on thiol-rich nanoframes

Linyi Bai,[a] Li Juan Tou,[a] Qiang Gao,[a] Purnandhu Bose,[a] Yanli Zhao*[,a,b]

[a]Division of Chemistry and Biological Chemistry, School of Physical and Mathematical Sciences, Nanyang Technological University, 21 Nanyang Link, Singapore 637371. E-mail: zhaoyanli@ntu.edu.sg

[b]School of Materials Science and Engineering, Nanyang Technological University, 50 Nanyang Avenue, Singapore 639798

1. General information

All reagents and solvents were purchased from Sigma-Aldrich and used as per received without further purifications. Fourier transform infrared (FT-IR) spectra were collected with an SHIMADZU IR Prestige-21 spectrometer. Samples were packed firmly to obtain transparent films. Thermogravimetric analyses (TGA) were performed on a TGA 500 thermogravimetric analyzer by heating the samples at 20 ºC min^{-1} to 900 ºC in a nitrogen atmosphere (60 mL min^{-1}). Powder X-ray diffraction (XRD) studies were performed on a SHIMADZU XRD-6000 Labx diffractometer, using Cu-Ka radiation (λ = 1.5418 Å) over 2θ range of 2.5°−40°, 40 keV, and 30 mA with a scanning rate of 0.02° s^{-1} (2θ) at room temperature. X-ray photoelectron spectroscopy (XPS) was performed with a Phiobos 100 spectrometer using Mg X-ray radiation source (SPECS, Germany) for wide range and high resolution scans at 12.53 kV. The XPS samples were coated on a conductive carbon tape, which was then fixed on aluminum XPS holder. TEM images were collected from a JEM-1400 transmission electron microscope (JEOL) operated at 100 kV. TEM grids were treated with oxygen plasma in a Harrick plasma cleaner/sterilizer for 60 s to clean the dust on the surface. The TEM grids were then placed in contact with the sample solution. A filter paper was used to wick off the excess solution on the TEM grid, which was then dried in air for 30 min. SEM images were collected on a field emission JSM-6700F (JEOL) operated at 10 kV. Gas sorption analyses were conducted using Quantachrome Instruments Autosorb-iQ (Boynton Beach, Florida USA) with extra-high pure gases.

2. Experimental section

2.1 Preparation of HKUST-1 nanocrystals

Benzene-1,3,5-tricarboxylic acid (H_3BTC, 4.2 mg, 0.02 mmol) was dissolved in a mixture of ethanol (25 mL) and deionized water (25 mL) under ultrasonic wave conditions. One equivalent of ammonia with respect to H_3BTC was added under stirring to give a clear solution. Next, $Cu(NO_3)_2 \cdot 3H_2O$ (0.3 mL, 0.1M) was added to the reaction mixture. The reaction mixture was stirred for 30 min. After which, blue precipitates were collected by centrifugation (2000rpm, 10 min) and then washed with ethanol for three times.

2.2 Preparation of NF-DMSA

Meso-2,3-dimercaptosuccinic acid (DMSA, 0.91 g, 5 mmol) was dissolved in a mixture of ethanol and water (v:v = 9:1, 50 mL). The HKUST-1 (0.5 g) powder in ethanol (50 mL) was added. An appropriate amount of tetra-*n*-butylammonium bromide (TBAB) surfactant was added to the mixture solution under stirring. The reaction was then placed to a thermal oven at 120 °C for 72 h, followed by cooling down to room temperature. Subsequently, an aqueous mixture (50 mL) of 25% NH_3H_2O (commercial) and 0.2 M NaOAc (v:v = 9:1) was added, and the reaction mixture was stirred for overnight. Some white powders in slight blue solution were observed. The white products were isolated by centrifugation (1000 rpm, 10 min) and washed with ethanol for three times.

2.3 Preparation of NF-DMSA

Dimercaptosuccinic sodium (DMSS, 1.13 g, 5 mmol) was dissolved in a mixture of ethanol and water (v:v = 9:1, 50 mL). The powder of HKUST-1 (0.5 g) in ethanol (50 mL) was added. An

appropriate amount of tetra-*n*-butylammonium bromide (TBAB) surfactant was added to the mixture solution under stirring. The reaction was placed to a thermal oven at 120 °C for 72 h, followed by cooling down to room temperature. Subsequently, the reaction was treated with the same base solution as abovementioned and kept stirring for overnight. The white products were isolated by centrifugation (1000 rpm, 10 min) and washed with ethanol for three times.

2.4 SEM monitoring and analysis of nanoframes

Alcohol solutions of $Zn(NO_3)_2$, $Zr(NO_3)_4$ and $Cu(NO_3)_2$ were prepared with 0.1 mM concentration. Next, DMSA powder was added into these solutions under stirring, and then the mixtures were placed into an oven for solvothermal reaction overnight. Some solids were formed during this process, and could be obtained by centrifugation and washing with ethanol for 3 times. Then, the dispersion in ethanol was dropped on the Si wafer, which was observed by SEM.

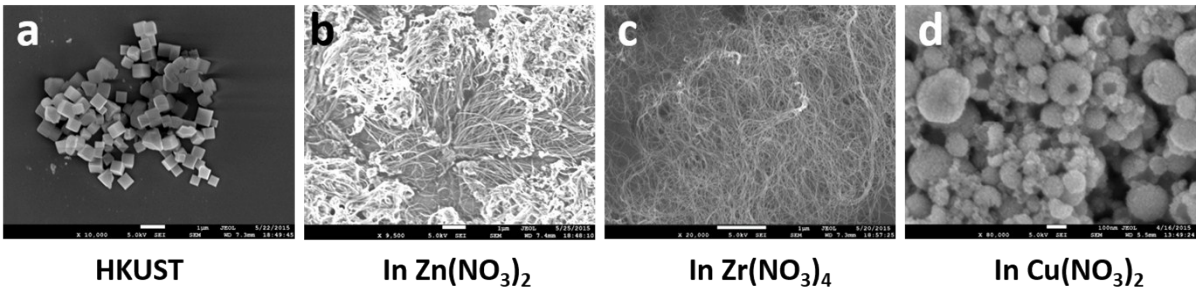

Figure S1. SEM images of (a) HKUST-1, and (b-d) products formed by adding DMSA to different solutions containing various metal ions.

As shown in Fig. S1, some linear nanowires were observed after the assembly of DMSA with Zn^{2+} and Zr^{4+}. In the presence of Cu^{2+}, however, there were spherical nanoparticles with the diameter of 100±10 nm formed after the process of assembly. Thus, different metal ions could have different influence on the assembly with DMSA. HKUST-1 was chosen as the supporting template to regulate the morphology of the final nanoframes.

In the subsequent morphology optimization of nanoframes, it was found that the DMSA nanoparticles prefer to grow on the edge of cubic HKUST-1 nanoparticles and gradually cover the whole surface of cubic HKUST-1 nanoparticles as shown in Fig. S2. After the assembly process, the diameter of DMSA nanoparticles was estimated to be ~100 nm, which is consistent with the size of independently grown nanoparticles without a template. Upon the treatment of base, central cubic object was etched off, leaving a hollow cubic cover of DMSA. The DMSA nanoparticles on the cover could be clearly seen in the TEM images.

When using DMSS, the formation of nanoframes showed a similar outcome, having preferable growth of DMSS nanoparticles on the edge of HKUST-1. The slight difference is that DMSS performed an in-situ accumulation after growing on the edge, instead of forming a cover. After 3 days, the final diameter of DMSS nanoparticles increased to ~210±15 nm.

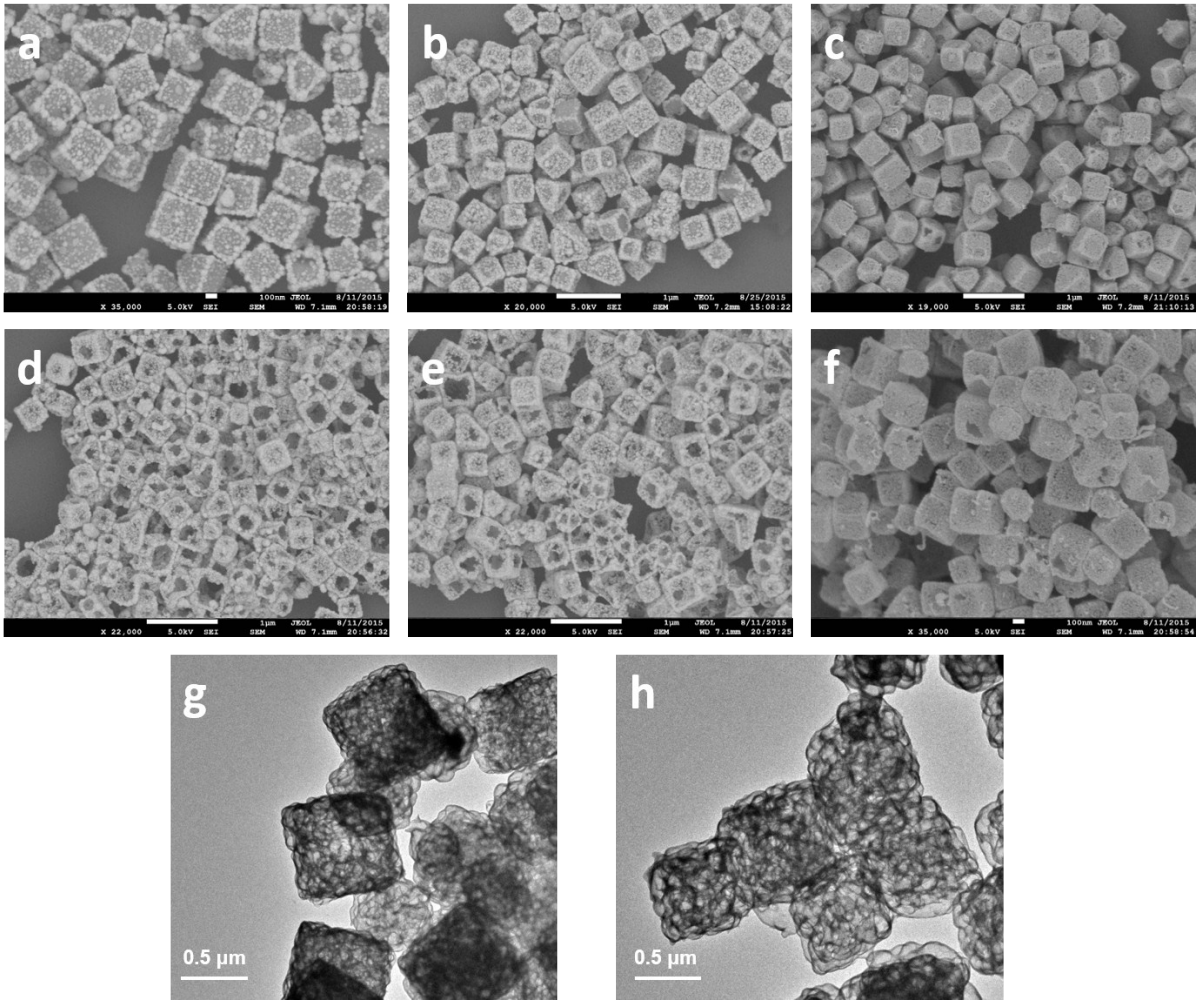

Figure S2. SEM and TEM images for monitoring NF-DMSA in different stages: (a-c) SEM images of products in solvothermal reaction for 24h, 48h and 72h, respectively; (d-f) SEM image of NF-DMSA samples collected from (a-c) after etching; (g,h) TEM images of NF-DMSA samples after etching.

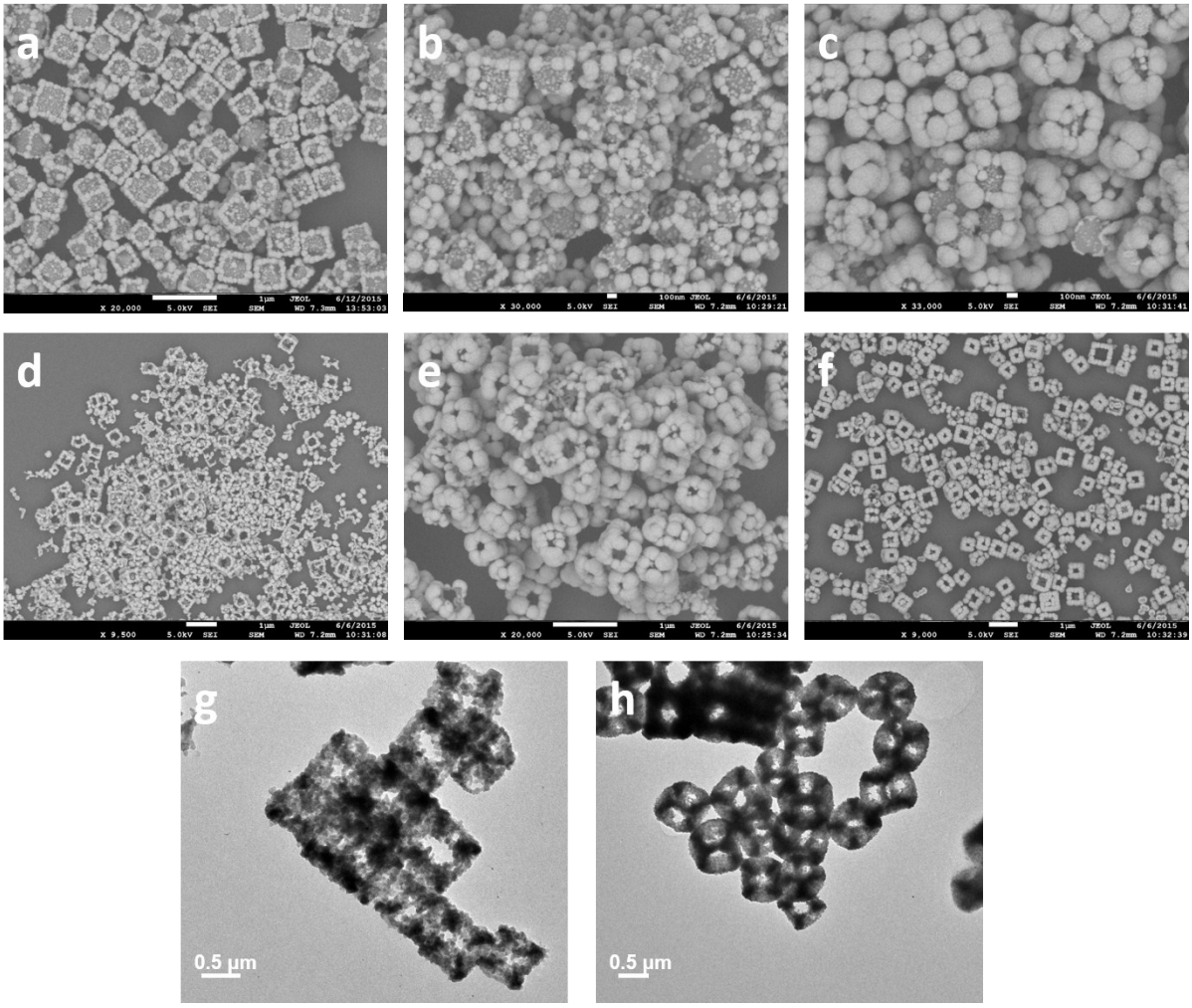

Figure S3. SEM and TEM images for monitoring NF-DMSS in different stages: (a-c) SEM images of products in solvothermal reaction for 24h, 48h and 72h, respectively; (d-f) SEM images of NF-DMSS samples collected from (a-c) after etching; (g,h) TEM images of NF-DMSS samples after etching.

3. Physical characterizations

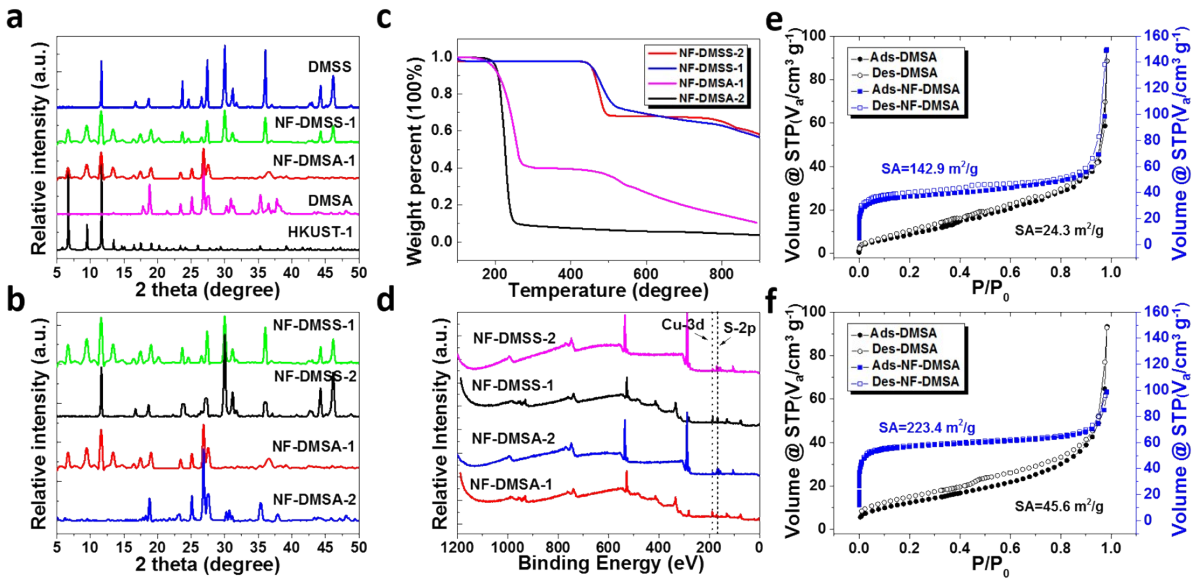

Figure S4. (a,b) Powder XRD patterns, (c) TGA, and (d) XPS spectra of the nanoframes in the growth process (R-1) and final product (R-2). (e,f) N_2 adsorption/desorption isothermal curves for NF-DMSA and NF-DMSS as compared with DMSA and DMSS powders. STP: standard temperature and pressure.

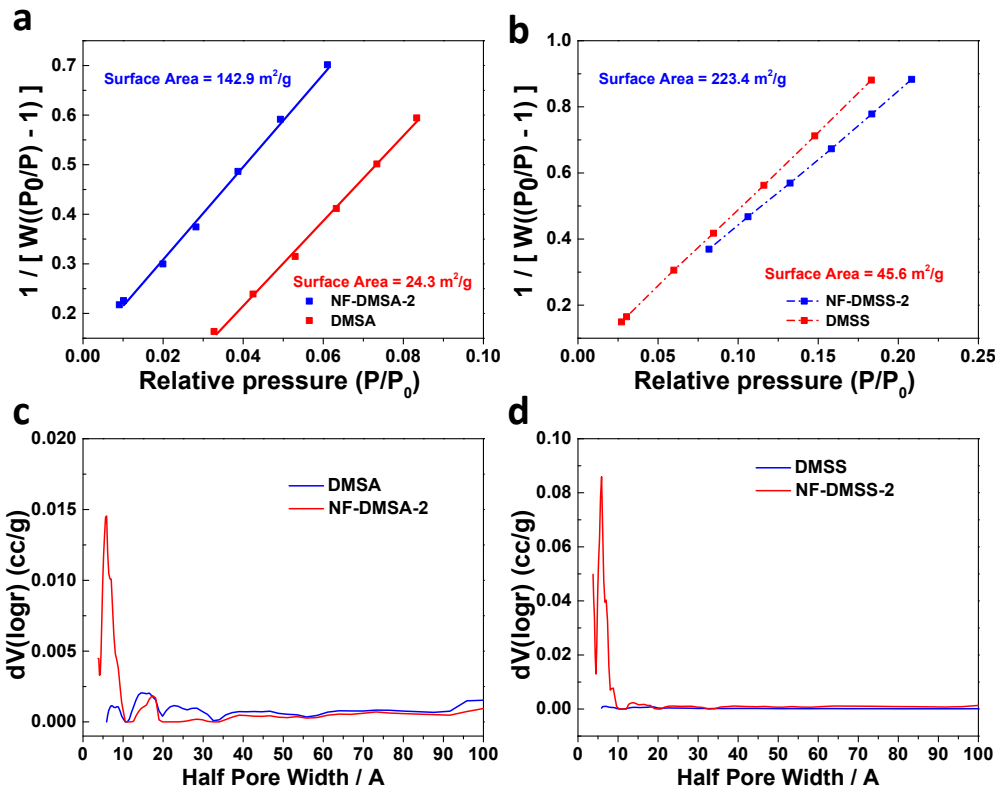

Figure S5. (a,b) BET surface areas and (c,d) pore-size distributions of DMSA, DMSS, NF-DMSA and NF-DMSS based on experimental N_2 adsorption/desorption isotherms using the nonlocal density functional theory (NLDFT).

Table S1. Statistics for micropores and mesopores based on *t*-plot method.

Item	Micropore SA[a] (m^2 g^{-1})	External SA[a] (m^2 g^{-1})	Total Pore Volume[b] (cc g^{-1})	Micropore Volume[a] (cc g^{-1})
DMSA	0	24.3	0.223	0
NF-DMSA-2	111.92	31.0	0.238	0.044
DMSS	0	45.6	0.232	0
NF-DMSS-2	170.68	52.7	0.239	0.056

The data were determined by N_2 adsorption/desorption isotherms at 77 K. [a] calculated by the *t*-plot method, where the contribution points were from 0.35 to 0.5 in P/P_0; [b] calculated by the point of the highest adsorption. SA = Surface Area.

4. Detection of heavy metal ions

4.1 Detection procedure

The thin films of NF-DMSA and NF-DMSS were obtained by directly dropping the dispersion of NF-DMSA and NF-DMSS on the transparent glass substrate and then keeping them at room temperature for solvent evaporation. Aqueous solutions containing heavy metal ions were prepared with a concentration of 0.01 mM. Here, $SnCl_4$, $Cd(NO_3)_2$, $PbCl_2$, As_2O_3, $Sb(NO_3)_2$, and $HgCl_2$ were used to prepare the solutions. Their practical photos were shown below. Then, the as-prepared films were immerged in these solutions, and the response time was recorded by a second chronograph.

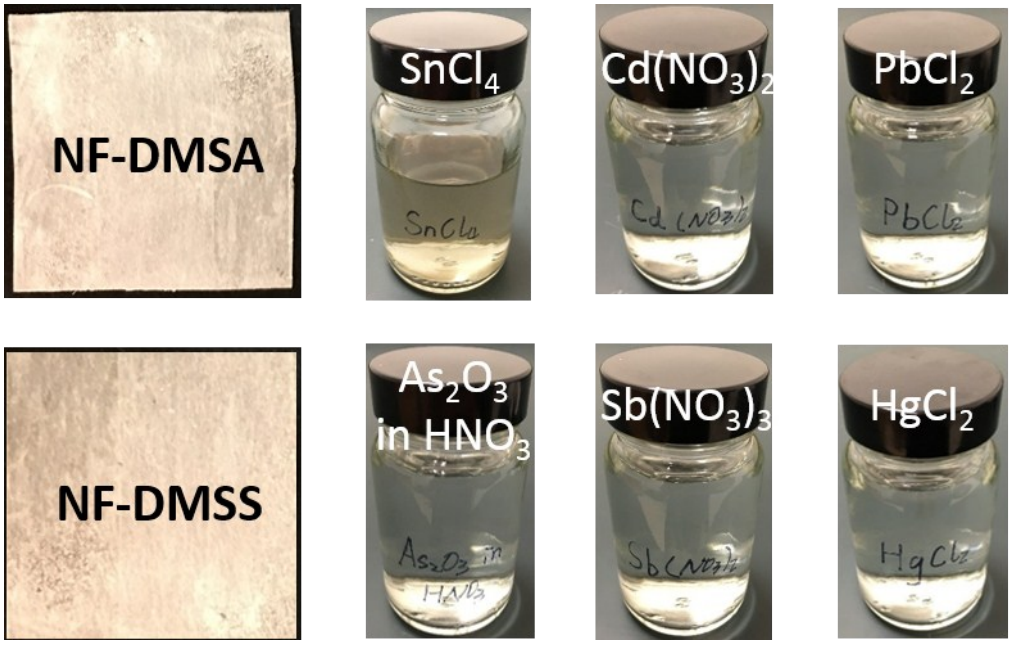

Figure S6. Practical photos of the films and the solutions containing heavy metal ions.

4.2 Colorimetric standard for comparison in different cases

CIE 1931 RGB color space and CIE 1931 XYZ color space were created by the International Commission on Illumination (CIE) in 1931.[S1] It represents all the chromaticity visible to human, and corresponding region is called the gamut of human vision. The gamut of all visible chromaticity on the CIE plot is the tongue-shaped figure shown in color.[S2] Wright and Guild's experiments were carried out using various primaries at various intensities, and they used a number of different observers. All of their results were summarized by the standardized CIE RGB color matching functions, obtained using three monochromatic primaries at standardized wavelengths of 700 nm (red), 546.1 nm (green) and 435.8 nm (blue).[S3] The color matching functions and primaries were settled by a CIE special commission after considerable deliberation.[S4]

Here, we defined the pure white point at [0.33, 0.33] as a standard, and then compared other colors with it. The contrast ratio was calculated by the distance between experimental point and the standard point. Based on the film colors observed in Figure 4a, several color values were achieved: [0.34, 0.37] is for NF-DMSA and $SnCl_4$, [0.37, 0.43] is for NF-DMSA and $Cd(NO_3)_2$, [0.55, 0.37] is for NF-DMSA and $PbCl_2$, [0.44, 0.34] is for NF-DMSA and As_2O_3 in HNO_3, [0.16, 0.03] is for NF-DMSA and $Sb(NO_3)_3$, and [0.17, 0] is for NF-DMSA and $HgCl_2$.

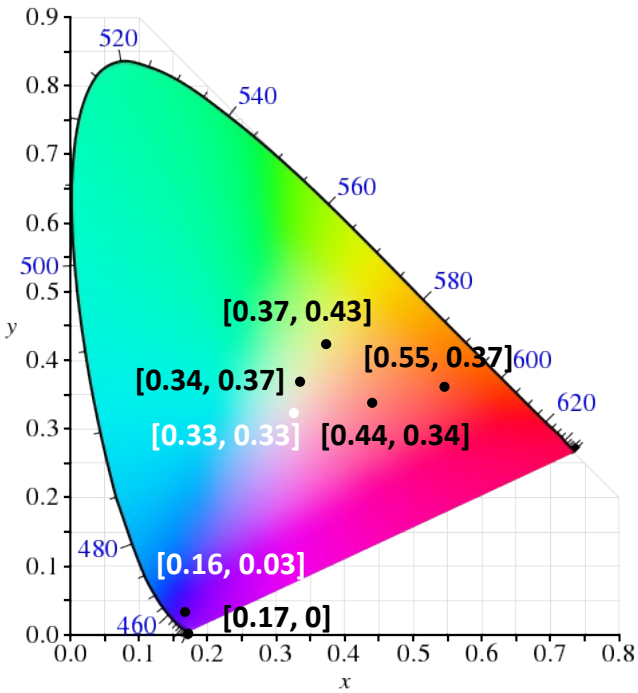

Figure S7. CIE 1931 color space chromaticity diagram. The standard point was defined at [0.33, 0.33]. [0.34, 0.37] is for NF-DMSA and $SnCl_4$, [0.37, 0.43] is for NF-DMSA and $Cd(NO_3)_2$, [0.55, 0.37] is for NF-DMSA and $PbCl_2$, [0.44, 0.34] is for NF-DMSA and As_2O_3 in HNO_3, [0.16, 0.03] is for NF-DMSA and $Sb(NO_3)_3$, and [0.17, 0] is for NF-DMSA and $HgCl_2$.

4.3 XPS spectra of NF-DMSA and NF-DMSS after detecting Sn(IV), Cd(III), Pb(II), As(III) and Sb(III)

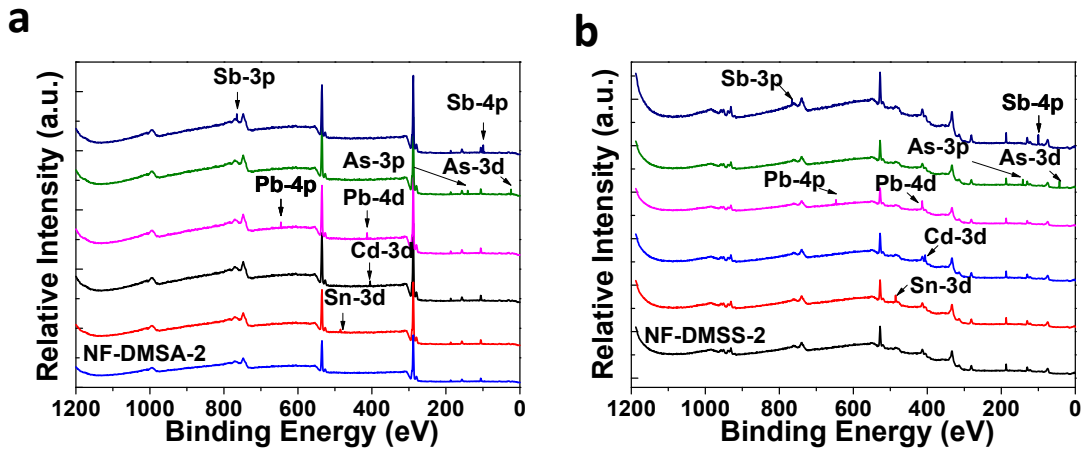

Figure S8. XPS spectra of (a) NF-DMSA and (b) NF-DMSS after interacting with $SnCl_4$, $Cd(NO_3)_2$, $PbCl_2$, As_2O_3 in HNO_3 and $Sb(NO_3)_3$.

In the XPS spectra, the specific peaks of different metal ions were easily observed in the final products, indicating an interaction between metal ions and thiol group in nanoframes. For the analysis of sulfur bonds, the peak S-2p could be observed in Fig. 3d, and there was a slight shift before and after treating nanoframes with heavy metal ions. This shift can be ascribed to the strong interaction caused by the complex effect between free thiol groups and heavy metal ions.

4.4 Powder XRD patterns

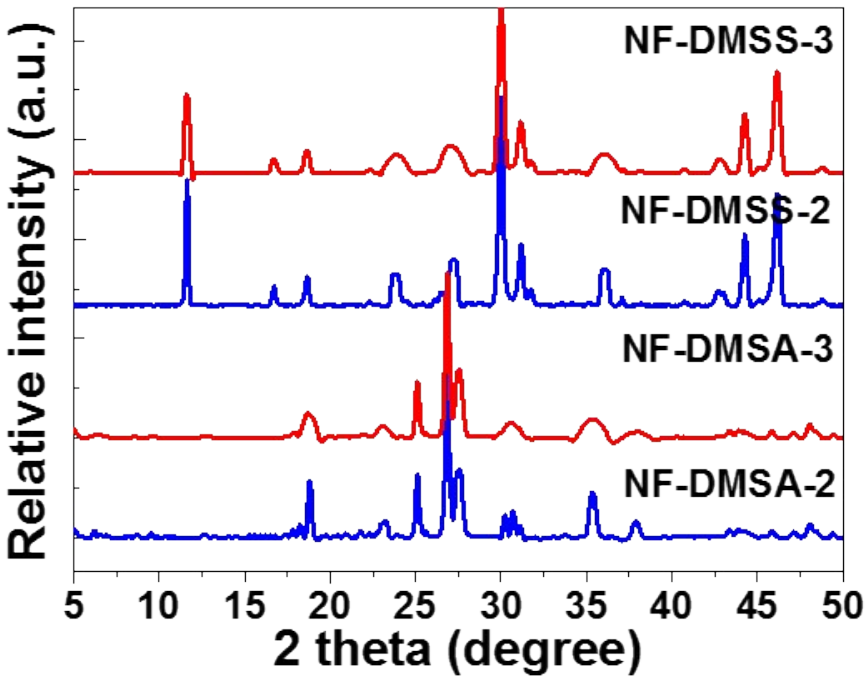

Figure S9. Powder XRD patterns of NF-DMSA and NF-DMSS before (blue) and after (red) the detection of heavy metal ions. The samples after the detection were dried under vacuum in the freeze dryer for 12 h before the XRD tests.

4.5 FTIR Spectra

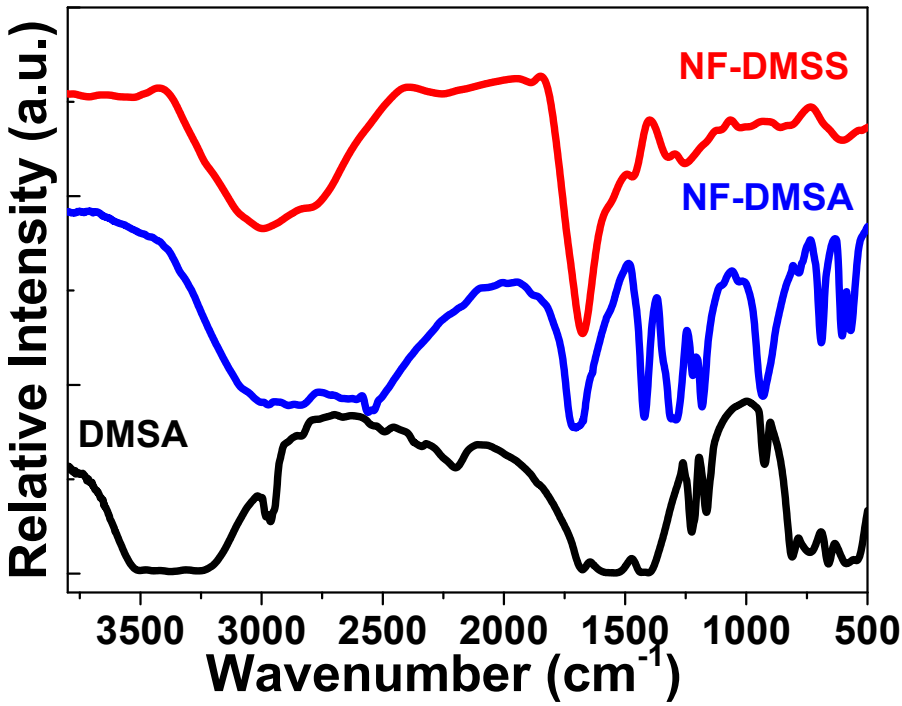

Figure S10. FTIR spectra of DMSA and two nanoframes, i.e. NF-DMSA and NF-DMSS. The FTIR spectrum of DMSA showed a broad stretching peak around 3200-3500 cm^{-1} for carboxylic group. There is no such specific peak observed from the two nanoframes, indicating there is no obvious free carboxylic unit in the nanoframes.

5. Sensing limit and recyclability studies

On account of similar sensing phenomenon, NF-DMSS was chosen to investigate its UV absorption changes upon metal ion treatments (Fig. S11). Considering the fact that more concentrated metal ion solutions can be detected easier, diluted metal ion solutions (diluting 0.1 mM by 10,100 and 1000 times) were used. The detection limits for different metal ions were calculated according to the linear relationship of the absorption changes and the concentrations, where the curve with the intensity 3 times higher than baseline was chosen as the standard. Based on the analysis of UV absorption changes, the detection limits of NF-DMSS for various heavy metal ions were evaluated to be ~1×10^{-4} mM, ~2×10^{-5} mM, ~7×10^{-6} mM, ~6×10^{-3} mM, ~3×10^{-3} mM, and ~8×10^{-3} mM for As^{3+}, Pb^{2+}, Hg^{2+}, Sb^{3+}, Sn^{4+} and Cd^{3+}, respectively.

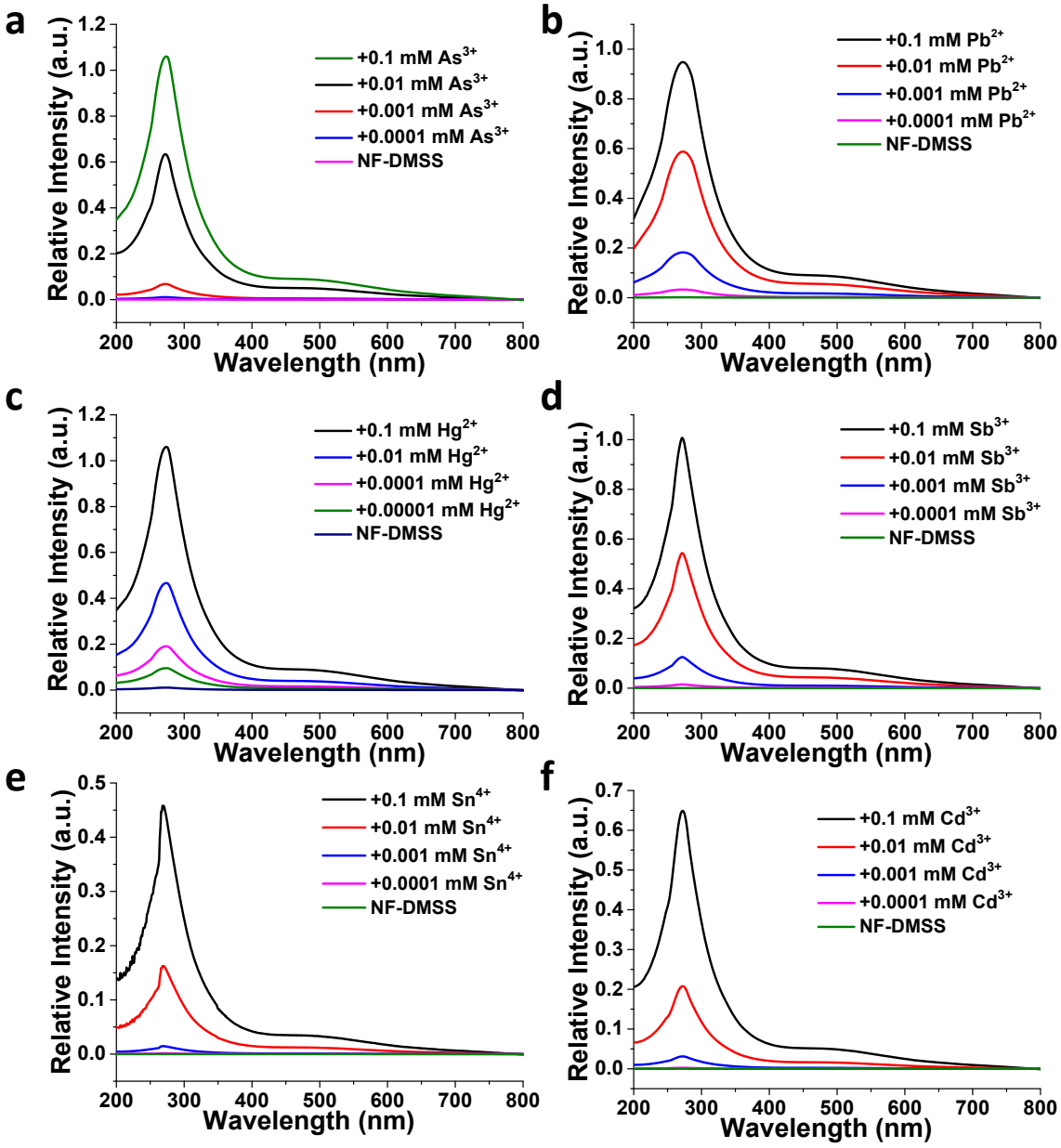

Figure S11. UV absorption changes of NF-DMSS nanoframe upon the additions of metal ion solutions.

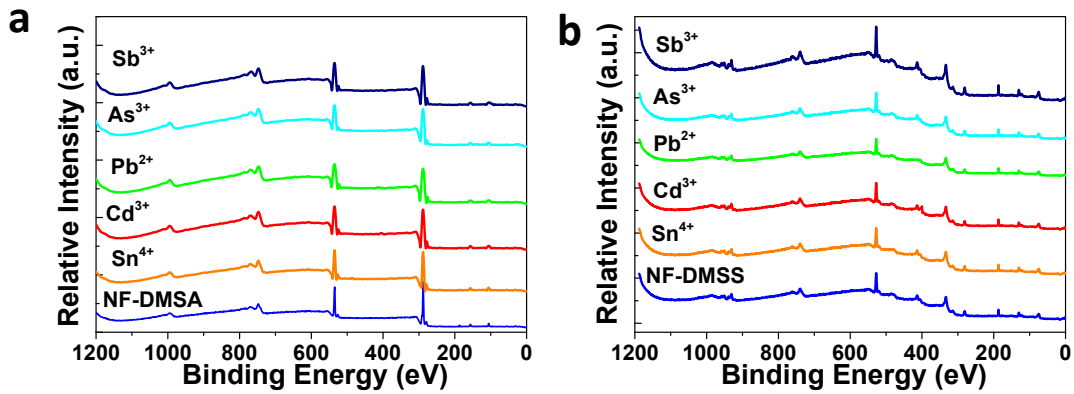

Figure S12. XPS spectra of two nanoframes complexed with metal ions after the EDTA treatments.

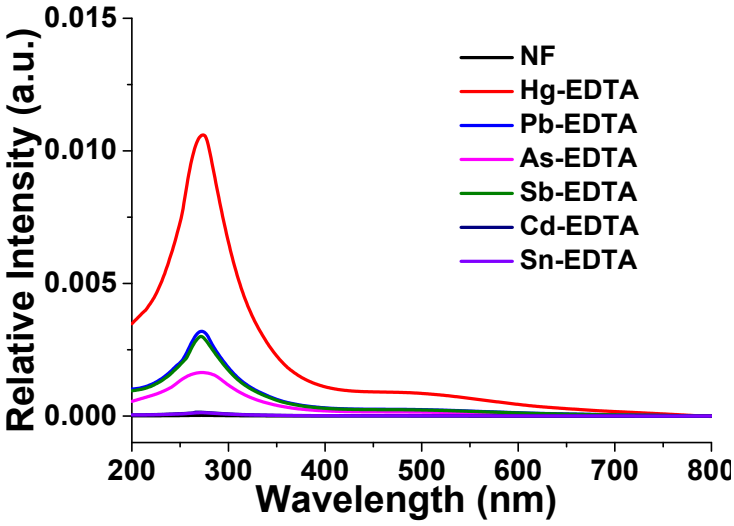

Figure S13. UV absorption changes of two nanoframes complexed with metal ions after the EDTA treatments.

For the recycling performance, we tried to use ethylenediaminetetraacetic acid (EDTA) to recover the nanoframes complexed with metal ions, and found that these nanoframes cannot be completely recovered to the initial state (Fig. S12 and S13). In the XPS spectra (Fig. S12), a few peaks from heavy metal ions were still observed after the EDTA treatment. When using UV absorption (Fig. S13), the significant UV peak was still observed after the EDTA treatment.

Overall, the present work shows two thiol-rich nanoframes that present an excellent capability of tracking heavy metal ions. Here, the detection performance of the nanoframes in mixed metal ion solution was concerned, since most polluted solutions contain normally a mixture of metal ions. Unfortunately, the present nanoframes were not suitable for distinguishing metal ion mixtures through a colorimetric sensing pathway. Colorless nanoframe films changed to deep color when interacting with As(III), Pb(II) and Hg(II), so that they cannot be used to respond to other ions. The selective response is applicable to single detection of metal ions, where the color difference can be easily observed. They may be some additional factors influencing the sensing capability, such as the ion strength, temperature and pH value. For example, some thermosensitive binding agents have a response to the changes of external temperature. In addition, the chelation of MOFs toward metal ions is another factor. The strong chelation effect may break the complexation between metal ions and the thiol-based binding agent, so that the detection performance will be seriously influenced. Herein, extensive development and efforts are highly desired for further addressing these challenges and promoting the detection capability of these nanoframes in follow-up studies.

References

S1. *CIE. Commission Internationale de l'Eclairage Proceedings. Cambridge University Press, Cambridge. 1931.*

S2. *Billmeyer and Saltzman. Principles of Color Technology 3rd Edition. Wiley-Interscience. 2000.* ISBN 0-471-19459-X.

S3. *J. Guild, The colorimetric properties of the spectrum. Philosophical Transactions of the Royal Society of London. 1931,* ***A230****: 149–187*

S4. *D. Malacara, Color Vision and Colorimetry: Theory and Applications. SPIE Press. 2002.* ISBN 0-8194-4228-3.